New Symmetry Breaking in Nonlinear Electroconvection of Nematic Liquid Crystals

Emmanuel Plaut, Werner Decker, Axel G. Rossberg, Lorenz Kramer, and Werner Pesch
Physikalisches Institut der Universität Bayreuth, D-95440 Bayreuth, Germany

Ahmed Belaidi and Roland Ribotta
Laboratoire de Physique des Solides, Université Paris-Sud, 91405 Orsay cedex, France
(Received 12 May 1997)

We report on a novel symmetry-breaking bifurcation in nematic liquid crystal convection in planarly aligned cells involving a homogeneous reorientation of the director. The resulting "abnormal rolls" explain a number of recent experimental observations in the nonlinear regime. [S0031-9007(97)04065-9]

PACS numbers: 83.70.Jr, 47.20.Ky, 47.20.Lz, 47.65.+a

Fluid layers driven far from equilibrium by an external stress can develop convection instabilities which break some of the underlying symmetries [1]. The most common case involves a bifurcation to stationary, periodically spaced convection rolls whose properties slightly above threshold (weakly nonlinear regime) can be described by an amplitude and a wave vector. Increasing the stress leads typically to further symmetry breakings, often involving changes of periodicity and/or time dependence. We report here on theoretical and experimental results concerning an unusual secondary symmetry breaking, which rather involves a spatially homogeneous stationary mode. To our knowledge it is the first time that in a pattern-forming nonequilibrium system such a transition has been identified.

This symmetry breaking occurs in the electroconvection of a nematic liquid crystal (EC) (for reviews on EC, see [2–4]). As compared to isotropic fluids a nematic is described by the additional director field $\mathbf{n} = (n_x, n_y, n_z)$, with $\mathbf{n}^2 = 1$, which represents the mean orientation of the elongated molecules. In EC a nematic layer (in the x, y plane) is sandwiched between two conducting plates, and the electric ac field of frequency ω is applied transversely (along $\hat{\mathbf{z}}$). In the common planar configuration the director is homogeneously oriented parallel to the plates in a fixed direction ($\hat{\mathbf{x}}$) by an appropriate treatment of their surfaces. The convection sets in for voltages V above a critical voltage $V_c(\omega)$. The conduction range, which is considered here, is limited from above by the crossover frequency ω_d. The main control parameter is V^2, and $\epsilon = (V^2 - V_c^2)/V_c^2$ defines the relative distance from onset. The roll diameter is of the order of the layer thickness (5–100 μm), and the anisotropy of nematics allows homogeneous patterns of very large aspect ratios (up to 500 rolls). The observation of the patterns rests on the periodic modulation of the director out of the x, y plane ($n_z \neq 0$).

Our experiments [5] were performed with the nematic Merck Phase 5, whose material parameters have all been measured, except for the absolute conductivity, or, equivalently, for the charge relaxation time $\tau_0 = \epsilon_0 \epsilon_\perp / \sigma_\perp$ [6]. At low frequencies one observes at threshold two degenerate variants of *oblique rolls* (OR), with wave vectors $\mathbf{q} = (q_c, \pm p_c)$ $(q_c, p_c > 0)$, and, beyond the Lifshitz frequency ω_L ($\simeq 0.8/\tau_0$) *normal rolls* (NR), with $\mathbf{q} = (q_c, 0)$, i.e., the roll axis normal to the anchoring direction $\hat{\mathbf{x}}$ [7]. Conventional NR can exhibit only point defects (dislocations). OR break the reflection symmetry $y \longrightarrow -y$ and thus can show in addition line defects (grain boundaries) separating domains with wave vectors (q, p) ("zig") and $(q, -p)$ ("zag") [8]. In Figs. 1(a) and 1(b) typical grain boundaries along $\hat{\mathbf{x}}$ and $\hat{\mathbf{y}}$ are shown.

However, surprisingly, in an apparently NR structure, line defects have been observed too. They are typically found in two situations:

(i) Starting in the low-frequency OR regime near threshold, the angle between the roll axis and $\hat{\mathbf{y}}$ is found to systematically decrease when ϵ is increased, and may even reach zero. In this process the grain boundary of Fig. 1(b) is transformed into the wall of Fig. 1(c). That the two domains on either side of the wall are not equivalent becomes more evident by further increasing ϵ. Indeed, one then observes the branching of an additional wave vector $(k_x, +k_y)$ on the right side, and $(k_x, -k_y)$ on the left side [Fig. 1(d)].

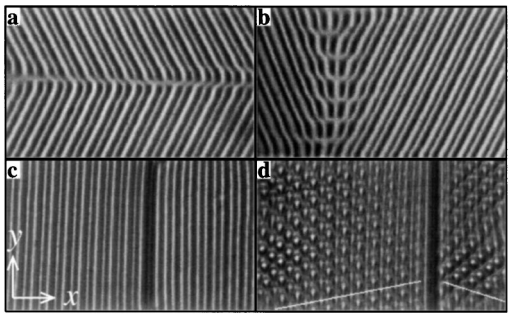

FIG. 1. Representative snapshots of the experimental evolution of electroconvection in a cell of thickness 5 μm, at $\omega\tau_0 = 0.3$. (a), (b): Zigzag structures near threshold ($\epsilon \simeq 0.02$), with "horizontal" and "vertical" grain boundaries. (c): Wall at $\epsilon \simeq 0.40$ originating from the grain boundary of (b). (d): Varicose structures at $\epsilon \simeq 0.70$, originating from the structure (c). The two modulation directions are indicated by the white lines.

(ii) Starting with NR at some higher frequency, walls are directly created when ϵ gets beyond a critical value [8], whereas the overall optical structure remains apparently unchanged. Here too, at higher ϵ, two symmetry-degenerate bimodals appear on either side of the walls.

Only the walls roughly parallel to the rolls [Fig. 1(c)] are quasistatic, whereas walls with different orientations move rapidly and appear to be unstable [5].

The existence of a two-variant state of normal rolls indicates a new symmetry breaking. We shall name those rolls *"abnormal rolls"* (AR), a term introduced in the context of homeotropically aligned cells [9] for rolls with an optically detected symmetry breaking; see later.

AR cannot be understood by the standard weakly nonlinear approach where the roll structure is characterized unambiguously by its wave vector and the linear eigenvector at threshold. Thus a full nonlinear analysis of the standard nematohydrodynamic equations [2] is required. One has to solve coupled partial differential equations for the velocity field, the director field, and the electric potential. As compared with isotropic fluids, the intrinsic anisotropy generates nonlinearities up to quintic order in the velocity equation. Adapting the well-established Galerkin method [10], we expand all fields in a complete set of functions which fulfill the boundary conditions at the confining plates. We kept the normalization condition $\mathbf{n}^2 = 1$ as a separate equation. The resulting nonlinear system for the expansion coefficients is solved numerically with the Newton method in order to obtain the roll solutions. Afterwards, their stability is studied by a linearization of the Galerkin equations.

Our key result is presented in Fig. 2. It shows the amplitude n_y^H of a twist mode corresponding to a *homogeneous rotation* (i.e., independent of x, y) of the director in the x, y plane as a function of ϵ and p for roll solutions with $\mathbf{q} = (q_c, p)$. This rotation is symmetric with respect to the mid plane of the layer, and is largest there. At $p = 0$, n_y^H vanishes if ϵ is sufficiently small, in agreement with the predictions of the weakly nonlinear theory. The novel and striking feature is the pitchfork bifurcation at a secondary transition point $\epsilon = \epsilon_{\mathrm{AR}}$ to a state with $n_y^H \neq 0$ (at $p = 0$). In these AR the $y \mapsto -y$ symmetry is spontaneously broken without tilting of the rolls. We found in addition that the amplitude of the (periodic) n_z component, which increases like $n_z \sim \sqrt{\epsilon}$ for small ϵ, as expected from the weakly nonlinear theory, remains nearly constant for $\epsilon \geq \epsilon_{\mathrm{AR}}$. For $p \neq 0$ the director "prefers" to rotate towards the axis of the rolls: e.g., $n_y^H < 0$ for $p > 0$ [lower sheet in Fig. 2]. However, for small positive p there also exist solutions with $n_y^H > 0$, which are only sketched in Fig. 2. They become quickly unstable, but in the unstable range one expects them to connect to the lower ($n_y^H < 0$) branch by an S-shaped curve (for fixed $\epsilon > \epsilon_{\mathrm{AR}}$) passing through the point $n_y^H = 0, p = 0$. Thus two overlapping sheets of stable rolls are attached to the normally oriented AR.

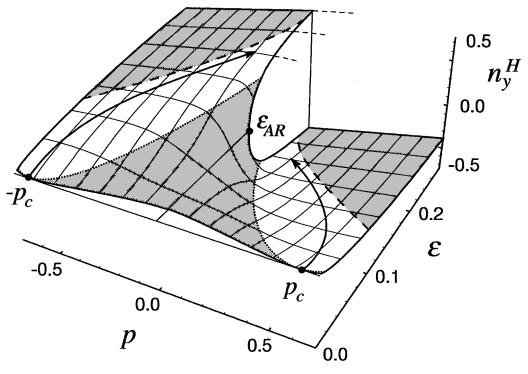

FIG. 2. Amplitude n_y^H of the twist mode in roll patterns of wave vector $\mathbf{q} = (q_c, p)$, as a function of p and ϵ at $\omega\tau_0 = 0.3$ (parameters of phase 5). Unstable regions in gray (Eckhaus boundary dotted, bimodal varicose boundary dashed). Arrows: Sketch of the experimental evolution of $p(\epsilon)$. In the experiments also q evolves with ϵ, which leads to quantitative changes of the diagram.

From a close inspection of the destabilizing mode, we identified two types of mechanisms responsible for the bifurcation NR $\longrightarrow$ AR, i.e., for the amplification of n_y^H fluctuations. Firstly, a small rotation n_y^H of the director excites, by coupling to the velocity and director fields of the NR, a spatially periodic velocity field parallel to the axis of the rolls ($v_y \propto e^{iqx}$), and a spatially periodic n_y field ($n_y \propto e^{iqx}$). These two fields then reinforce the initial director rotation. This mechanism essentially involves some velocity-director coupling terms, i.e., the α_2 terms in the viscous stress tensor, and the related α_2 terms in the director equation (backflow effects) [2]. Secondly, the spatially periodic velocity and director fields of the NR ($v_z, n_z \propto e^{iqx}$) directly renormalize the damping of n_y^H. In this renormalization, one can distinguish backflow effects, and an elastic contribution proportional to $k_{33} - k_{22}$, expressing the release of (nonlinear) bend by twist. This latter effect becomes important at high frequencies where q gets fairly large ("narrow rolls"). Some ingredients of these mechanisms have already been described in the literature for similar systems [11,12].

The relevance of the bifurcation diagram in Fig. 2 has been assessed by a stability analysis, and in Fig. 3 the results for rolls with $\mathbf{q} = (q_c, 0)$ are shown in the ϵ, ω plane. The limiting curves of the unstable regimes (in gray) will now be discussed. For $\omega < \omega_L$, where the primary bifurcation is to OR, NR are unstable near threshold ($\epsilon \simeq 0$) against long-wavelength undulations along the roll axis ("zigzag" instability). This instability is driven by the resonant superposition of two symmetric modes $\mathbf{q} \pm \mathbf{s}$ with $\mathbf{s} \perp \mathbf{q}$, i.e., $\mathbf{s} = s_y \hat{\mathbf{y}}$ [13]. The mechanism gets less efficient in the AR, where the $y \mapsto -y$ symmetry is broken. Thus AR become stable when $|n_y^H|$ is large enough, for $\epsilon > \epsilon_{\mathrm{AR\,stab}}(\omega)$ (dotted line). When ϵ is increased further the AR are destabilized at $\epsilon_{\mathrm{BV}}(\omega)$ (dashed line), now by a short-wavelength instability with

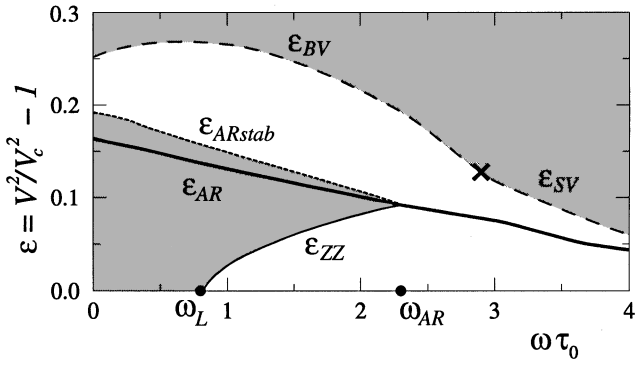

FIG. 3. Stability diagram for rolls in the normal direction ($p = 0$) in the ω, ϵ plane (unstable regimes in gray). ϵ_{AR} (thick line): NR $\rightarrow$ AR bifurcation. ω_L = Lifshitz frequency, ϵ_{ZZ} (thin line): Zigzag instability. $\epsilon_{\mathrm{AR\ stab}}$ (dotted line): Restabilization of the abnormal rolls. The upper dashed line is at low frequencies a short-wavelength varicose instability (ϵ_{BV}) that transforms into a long-wavelength skewed-varicose instability (ϵ_{SV}) at $\omega\tau_0 \simeq 2.8$ ($\times$).

a new wave vector $|\mathbf{k}| \simeq q_c$ roughly parallel to the homogeneous part of the in-plane director (n_x^H, n_y^H) in the AR. This mechanism has been described before for OR [12], but it also applies to the AR, which are continuously attached to the OR (see, e.g., the lower sheet of Fig. 2). The resulting strongly asymmetric bimodal [Fig. 1(d)] has also been called a "bimodal varicose," and the secondary wave vector $\mathbf{k}$ a "dual" of $\mathbf{q}$ [14,15].

In an intermediate frequency range $\omega_L < \omega < \omega_{\mathrm{AR}}$, NR are stable for $\epsilon \leq \epsilon_{\mathrm{ZZ}}(\omega)$ (solid line). At ϵ_{ZZ} a zigzag instability also develops [7], which derives continuously from the zigzag instability at low ω: $\epsilon_{\mathrm{ZZ}}(\omega) \longrightarrow 0$ for $\omega \longrightarrow \omega_L$. Above ϵ_{ZZ} the situation is analogous to the low-frequency regime, i.e., one gets stable AR for $\epsilon > \epsilon_{\mathrm{AR\ stab}}$. When ϵ is increased further the AR experience the varicose destabilization at ϵ_{BV} as before.

The stability limits $\epsilon_{\mathrm{AR}}, \epsilon_{\mathrm{AR\ stab}}$ and ϵ_{BV} decrease as functions of ω [Fig. 3]. Above the frequency ω_{AR}, where ϵ_{ZZ}, $\epsilon_{\mathrm{AR\ stab}}$ meet the line ϵ_{AR}, the bifurcation NR $\longrightarrow$ AR occurs *in the stable range*. Along the varicose line $\epsilon_{\mathrm{BV}}(\omega)$, the modulation wave vector $\mathbf{s} = \mathbf{k} - \mathbf{q}$ approaches zero with increasing ω, whereas the ratio s_y/s_x stays finite ($s_y/s_x \simeq \pm 2.7$). Above $\omega\tau_0 \simeq 2.8$ [cross in Fig. 3], the varicose instability thus becomes a long-wavelength modulational instability of the skewed-varicose type [13].

Now we come to the stability regimes of OR. In the typical example of Fig. 2, for $q = q_c, \omega < \omega_L$, the unstable ranges are shown in gray. At $\epsilon \simeq 0$ only the rolls with $p \simeq \pm p_c$ are stable. With increasing ϵ the stable ranges, limited by an Eckhaus instability (dotted line in Fig. 2, which connects parabolically to $\epsilon = 0, p = \pm p_c$), grow. The stable roll ranges are limited from above by the bimodal instability (dashed line in Fig. 2). At large $|p|$ this line bends back and connects to the Eckhaus line (not shown). With increasing ω the qualitative features of the stability regimes are changed at first only for small ϵ. The lower part (small ϵ) of the central gray region in Fig. 2 shrinks in accordance with the decrease of p_c. At $\omega = \omega_L$ it lifts off the p axis and for $\omega > \omega_L$ there remains an unstable bubble extending in the ϵ, p plane from ϵ_{ZZ} to $\epsilon_{\mathrm{AR\ stab}}$ and between $\pm p_{\max}$. For $\omega \longrightarrow \omega_{\mathrm{AR}}$ the bubble shrinks to zero.

In the following we discuss the experimental evidences for the new scenarios involving AR. The direct observation of a homogeneous n_y distortion in the planar configuration is difficult. The optical axis of the uniaxial nematics is the director. Maximal optical contrast is achieved in extraordinary light, when the polarization of the light is parallel to the director at the plates $\hat{\mathbf{x}}$. The polarization then follows adiabatically any n_y excursion in the bulk and exits parallel to $\hat{\mathbf{x}}$ again, as long as n_y varies slowly over a wavelength of the light (Mauguin's principle). Therefore only n_z is monitored, whereas the n_y distortion has almost no effect on the propagation of the rays.

However, the AR can be evidenced when starting from a polydomain configuration [Fig. 1(b) and 1(c)]. On either side of the grain boundary one has opposite n_y^H orientations. The resulting strong n_y gradients inside the grain, coupled to a localized peak of n_z, explain the observed optical contrast of the wall. The bimodal patterns in Fig. 1(d) then obviously result from the destabilization of AR at $\epsilon = \epsilon_{\mathrm{BV}}$ (see Fig. 3). Using the material parameters [6], and for the experimental wave vector $\mathbf{q}(\epsilon)$, we have calculated the various transition points. We found $\epsilon_{\mathrm{AR\ stab}} = 0.18$ and $\epsilon_{\mathrm{BV}} = 0.42$ for the situation depicted in Fig. 1 ($\omega\tau_0 = 0.3$). In the experiments, AR were selected spontaneously only for $\epsilon \gtrsim 0.40$ (for smaller ϵ, the system remained in an OR state). The transition to homogeneous bimodal occurred at $\epsilon_{\mathrm{BV}} \simeq 0.50$. The theoretical value for the angle between $\hat{\mathbf{x}}$ and the dual wave vectors $\mathbf{k}$ ($\pm 83°$) is in good agreement with the experimental one ($\pm 81°$). A direct experimental proof of the in-plane rotation of the director seems nevertheless desirable, possibly with the help of special optical methods (see [16]).

In addition to the direct observation of walls at high frequency in AR (ii), there is other evidence for the qualitative changes expected from theory when the frequency crosses ω_{AR}. Experiments in the nematic MBBA have indeed shown a crossover from a zigzag to a skewed-varicose destabilization for rolls in the normal direction at $\omega \simeq 1.0/\tau_0$ [17]. This agrees quite well with our theoretical value for MBBA, $\omega_{\mathrm{AR}} = 1.1/\tau_0$. The skewed-varicose instability is known to lead to the generation of dislocations in striped patterns, and indeed beyond ω_{AR} and (presumably) ϵ_{AR} various kinds of (dynamic) defect structures were detected [8,17].

AR also explain experimental observations in EC in homeotropically oriented cells (director prepared perpendicular to the confining plates), where we have

numerically identified the secondary n_y^H bifurcation too [18]. In this geometry, EC typically arises after an electric Fréedericks transition. The in-plane direction $\hat{\mathbf{x}}$ of the director field before EC is either spontaneously chosen, or determined by a horizontal magnetic field. In contrast to the planar case, the polarization of extraordinary light is now determined by the in-plane director in the bulk. Therefore it is clear that in AR the maximal optical contrast requires a polarization of light not parallel to $\hat{\mathbf{x}}$, as observed in [9]. Also, optical effects similar to that shown in Fig. 1(c), i.e., rolls in the normal direction separated by dark bands (horizontal and vertical), have been seen quite recently [19,20]. Further bifurcations in these structures [see Fig. 9(b) of [20]], which show some similarities to the one shown in Fig. 1(d), underscore the fact that the $y \mapsto -y$ symmetry has been broken due to a in-plane rotation of the director.

A more detailed presentation of the mechanisms involved in the transition to AR and of the stability diagram, which can also be captured by an extended weakly nonlinear analysis as introduced in [11], will be presented elsewhere. In addition, a normal-form type analysis in terms of a phase diffusion equation coupled to the n_y^H mode, applicable in particular in the neighborhood of the highly degenerate bifurcation point at ω_{AR}, is in progress. Finally, the role of the dynamics of defects in the AR is under investigation.

In conclusion, we have found in the best-studied model system for anisotropic convection a novel symmetry breaking through nonlinear coupling of multiple fields, which had been overlooked since it is hidden in the optical pattern. It appears to be generic in nematic electroconvection, since it develops in planar and in homeotropic geometry. It is also decisive for the understanding of EC in the higher-frequency ($\omega > \omega_d$) dielectric regime [2–4], in particular of the "chevrons." Moreover, preliminary calculations show that the same symmetry breaking should also occur in thermoconvection in nematics.

Our results demonstrate the importance of the in-plane director degree of freedom, and open the way for an understanding of well known, but as yet not understood phenomena in the strongly nonlinear regime of nematic convection. We mention oscillating bimodal structures, defect lattices, and the strongly chaotic (or turbulent) dynamic scattering regime. Some experimental results concerning the defect lattice as well as a description of weakly chaotic states will be presented elsewhere [5].

Financial support by the Deutsche Forschungsgemeinschaft (DFG-Kr690/4-4), DRET Contract No. 94/136, and the TMR network "Patterns, Noise and Chaos" (FMRX-CT96-0085) is gratefully acknowledged.

[1] M. C. Cross and P. C. Hohenberg, Rev. Mod. Phys. **65**, 851 (1993); P. Manneville, *Dissipative Structures and Weak Turbulence* (Academic, New York, 1990).

[2] S. Chandrasekhar, *Liquid Crystals* (Cambridge University Press, Cambridge, 1992); P. G. de Gennes and J. Prost, *The Physics of Liquid Crystals* (Clarendon, Oxford, 1993).

[3] For reviews of EC, see I. Rehberg, B. L. Winkler, M. de la Torre, S. Rasenat, and W. Schöpf, Adv. Solid State Phys. **29**, 35 (1989); S. Kai and W. Zimmermann, Prog. Theor. Phys. Suppl. **99**, 458 (1989); Ref. [4].

[4] L. Kramer and W. Pesch, in *Pattern Formation in Liquid Crystals*, edited by A. Buka and L. Kramer (Springer-Verlag, New York, 1996).

[5] A. Belaidi, Ph.D. thesis, Orsay, 1997; A. Belaidi and R. Ribotta (to be published).

[6] At 30 °C, phase 5 has elastic constants $= (k_{11}, k_{22}, k_{33}) = (9.8, 4.6, 11.4)\,10^{-12}$N; viscosities $= (\alpha_1, \alpha_2, \alpha_3, \alpha_4, \alpha_5, \alpha_6) = (-39.0, -109.3, 1.5, 56.3, 82.9, -24.9) \times 10^{-3}\mathrm{N\,s\,m^{-2}}$; dielectric constants $= (\epsilon_\parallel, \epsilon_\perp) = (5.11, 5.29)$; conductivity ratio $= \sigma_\parallel/\sigma_\perp = 1.7$. See H. H. Graf, H. Kneppe, and F. Schneider, Mol. Phys. **77**, 521 (1992); M. Treiber, N. Eber, A. Buka, and L. Kramer, J. Phys. (Paris) **7**, 649 (1997). The conductivity perpendicular to the director $\sigma_\perp$ determines primarily the frequency scale. We have adjusted $\sigma_\perp$ to $4.4 \times 10^{-8}\,(\Omega\,\mathrm{m})^{-1}$, which leads to $1/(2\pi\tau_0) = 150$ Hz. This matches the experimental crossover at $f_d = 600$ Hz to $\omega_d\tau_0 = 4$ from theory.

[7] R. Ribotta, A. Joets, and Lin Lei, Phys. Rev. Lett. **56**, 1595 (1986).

[8] A. Joets and R. Ribotta, J. Stat. Phys. **64**, 981 (1991); X. D. Yang, A. Joets, and R. Ribotta, in *Propagation in Systems Far from Equilibrium*, edited by J. E. Wesfreid *et al.* (Springer-Verlag, Berlin, 1988).

[9] H. Richter, A. Buka, and I. Rehberg, in *Spatio-Temporal Patterns in Nonequilibrium Complex Systems*, edited by P. E. Cladis and P. Palffy-Muhoray (Addison-Wesley Publishing Company, Reading, MA, 1994).

[10] See, e.g., R. M. Clever and F. H. Busse, J. Fluid Mech. **65**, 625 (1974).

[11] A. G. Rossberg, A. Hertrich, L. Kramer, and W. Pesch, Phys. Rev. Lett. **76**, 4729 (1996).

[12] E. Plaut and R. Ribotta, Phys. Rev. E **56**, R2375 (1997).

[13] F. H. Busse, Rep. Prog. Phys. **41**, 1929 (1978).

[14] R. Ribotta and A. Joets, J. Phys. (Paris) **47**, 739 (1986).

[15] E. Plaut and R. Ribotta, Europhys. Lett. **38**, 441 (1997).

[16] M. Grigutsch, N. Klöpper, H. Schmiedel, and R. Stannarius, Mol. Cryst. Liq. Cryst. **262**, 283 (1993); H. Amm, R. Stannarius, and A. G. Rossberg (to be published).

[17] S. Nasuno, O. Sasaki, S. Kai, and W. Zimmermann, Phys. Rev. A **46**, 4954 (1992).

[18] A. Hertrich, Ph.D. thesis, Bayreuth, 1996.

[19] H. Richter, N. Klöpper, A. Hertrich, and A. Buka, Europhys. Lett. **30**, 37 (1995).

[20] S. Kai, K. Hayashi, and Y. Hidaka, J. Phys. Chem. **100**, 19 007 (1996).